Pattern formation in discrete cell tissues under long range filopodia-based direct cell to cell contact

Georgios Vasilopoulos and Kevin J. Painter*

Department of Mathematics and Maxwell Institute for Mathematical Sciences,
Heriot-Watt University,
Edinburgh, EH14 4AS, UK.
*Author for correspondence: K.Painter@hw.ac.uk

Abstract

Pattern formation via direct cell to cell contact has received considerable attention over the years. In particular the lateral-inhibition mechanism observed in the Notch signalling pathway can generate a regular periodic pattern of differential cell activity, and has been proposed to explain the emergence of patterns in various tissues and organs. The majority of models of this system have focussed on short-range contacts: a cell signals only to its nearest neighbours and the resulting patterns tend to be of fine-scale "salt and pepper" nature. The capacity of certain cells to extend signalling filopodia (cytonemes) over multiple cell lengths, however, inserts a long-range or non-local component into this process. Here we explore how long range signalling can impact on pattern formation. Specifically, we extend a standard model for Notch-like lateral inhibition to include cytoneme-mediated signalling, and investigate how pattern formation depends on the spatial distribution of signal from the signalling cell. We show that a variety of patterns can be obtained, ranging from a sparse pattern of single isolated cells to larger clusters or stripes.

Keywords: lateral inhibition; pattern formation; morphogenesis; cytoneme signalling; Delta-Notch interactions; juxtracrine models

1. Introduction

Determining the communication channels through which a cell population patterns and differentiates itself is central to understanding the development, homoeostasis, repair and pathogenesis of the tissues and organs of our bodies. Many early theories

invoked the concept of *morphogens*, chemical signalling molecules capable of directing the behaviour and differentiation of cells: for example, the seminal model of Turing [30] proposed that a system of reacting and diffusing molecules could form a spatially periodic pattern, and that this information offered a patterning blueprint; the French-flag model of Wolpert [34] posited that a non-uniform distribution of a morphogen could pattern a tissue via distinct differentiation paths being followed by cells according to the morphogen level. Numerous morphogens have been discovered, and their various modes of operation have been the source of considerable theory and speculation (e.g. see the review in [23]).

In many models, morphogen transport is explicitly or implicitly assumed to result from simple diffusion in the extracellular space: for example, in Turing's model diffusion is (surprisingly) the critical factor that breaks initial symmetry to create pattern; Crick [6] calculated that small(ish) molecules were (theoretically) capable of diffusing through tissues in timescales relevant for early embryonic processes. In recent years, a combination of theoretical modelling and experimental data have supported molecular diffusion as a potential morphogen transport mechanism (e.g. [35, 14]).

In certain signalling systems, however, the intercellular communication required for pattern formation can be achieved without extracellular diffusion, a particular well known example being the Notch system. This crucial signalling pathway is widely conserved throughout the animal kingdom and found to control/regulate a diverse range of processes in both developing and adult tissues [1, 10]. The Notch receptor and its ligands, the Delta/Serrate/Lag2 (DSL) family, are transmembrane proteins that require cell to cell contact due to their membrane-tethered nature: while diffusible forms of ligand exist, they do not appear to trigger signalling [12]. In other words, cell to cell signalling is achieved through a *direct and one-to-one* contact between a signaller cell and receiver cell, providing *juxtacrine signalling*. Diffusion, on the other hand, allows *paracrine* signalling: a secreting cell could signal many or all other cells in a population. Such direct signalling is by no means confined to the Notch signalling system, or receptor/ligand modes of communication: for example, cadherin adhesion molecules create cell-to-cell adhesive bonds that also provide sig-

2

nalling [33]; information can also pass directly from cell to cell via "gap-junction" tunnels between two membranes [16], allowing small molecules to pass directly from cytoplasm to cytoplasm.

In the context of developmental pattern formation Delta-Notch signalling is capable of operating a lateral-inhibition scheme [1, 10], where high receptor (Notch) activity in a receiving cell down-regulates its own ligand (Delta) activity, and hence its capacity to signal other cells (see Figure 1 (a)). Between two quasi-identical cells, stochastic fluctuations in their initial ligand and receptor activities will be steadily amplified, with one cell's ligand activity progressively downregulated to the extent that it cannot induce a similar reponse in the other: one cell "wins" and the other "loses", distinct signalling activities are displayed and the cells take alternate fates. In an array of cells, this juxtacrine-based mechanism of lateral inhibition can generate a fine-scale "salt and pepper" pattern of signalling activity (see Figure 1 (b)), and hence provide a potential mechanism for certain types of tissue patterning. Notch-based pattern formation has received intense scrutiny during many development processes, such as sensory bristle formation in the fruit-fly thorax [27, 1, 10]. These mechanosensory bristles develop from single sensory organ precursor (SOP) cells, which form at regular spaced intervals in an epithelial field through a Notch-Delta lateral inhibition process [27].

A number of mathematical models have been developed to explore juxtacrine-based signalling in patterning. Collier, Monk and others [5] devised a model for juxtacrine-based lateral inhibition that consisted of a network of coupled equations for the signalling activities of Delta and Notch in each cell. Juxtacrine signalling was incorporated via a cell's receptor activity depending on the ligand activity of its nearest neighbours, and the model was shown to reproduce the fine-grained patterning of a cell sheet. This framework has subsequently been adapted and extended in various directions, from more detailed analytical explorations to refined representation of the molecular interactions, or specific modelling of particular instances of pattern formation: as examples, we refer to [13, 18, 19, 31, 20, 32, 21, 8, 3, 29, 28, 17, 26, 2].

On initial reading, the "juxtacrine" labelling of Delta-Notch interactions suggests

strictly local communication, such that a cell can only signal to its nearest neighbours. Consequently, the length scales of any developing patterns is somewhat uncertain. For example, in the lateral-inhibition based model of [5], each cell signals only to its nearest neighbours and the corresponding pattern tends to a fine-scale form: a more-or-less alternating pattern of distinct signalling states (e.g. see an example in Figure 9 (a)). In contrast, the spacing between SOPs during bristle formation is somewhat larger, raising the question as to what coarsening factors could contribute to the process.

Many cells, even in highly packed epithelial layers, have a dynamic form that allows the extension of long membrane protrusions such as filopodia. In particular, much attention has focussed on the capacity of certain cells to extend long, oriented "signalling filopodia" – often referred to as cytonemes [22] – that can contact and directly signal to more distant cells, possibly up to $200\mu m$ (10s of cell lengths) away (e.g. see the reviews in [25, 9, 11]). Consequently, the directly-contactable neighbourhood of a cell may extend considerably beyond its nearest neighbours. In the context of Notch-Delta based SOP patterning, de Joussineau *et al* [7] found Delta expressed along filopodia puncta and, speculating that this may increase the range of lateral inhibition, showed that disrupting the protrusions resulted in a shorter spacing and over-expressed SOPs. More recently, Cohen *et al* [3] used a combined experimental/theoretical approach to show that the length and lifetime of the dynamic filopodia extended by bristle precursors correlated with the pattern and density of bristles. Beyond this role in lateral-inhibition based pattern formation, cytoneme- or filopodia-mediated cell to cell signalling has been associated to numerous processes in development: most frequently in drosophila, such as Dpp-regulated anterior/posterior border specification and hedgehog (Hh) delivery in the wing-disc, but also vertebrates (for example sonic hedgehog signalling in chick limb buds); we refer to [25, 9, 11] for reviews.

1.1. Outline

In this paper we consider the impact of long-range, direct contact signalling on the patterning of cellular tissues. We use the classic system of Delta-Notch signalling as a case study, extending the analytically convenient model of [5] to account for
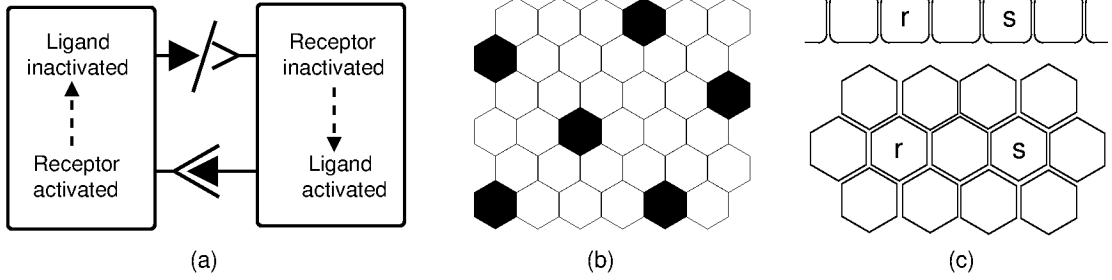
Figure 1: (a) Illustration of the Delta-Notch lateral inhibition mechanism, adapted from [5]. (b) Lateral-inhibition operating in a Juxtacrine signalling process is capable of creating a finely grained pattern of alternate cell fates. (c) The 1D and 2D geometries considered for the modelling. We note that for the two cells r and s we have $d_{r,s} = 2$.

non-local interactions. Specifically, we construct a general form in which each cell creates a signalling net, contacting other cells in some non-local neighbourhood. In its general form the equations can be adapted to include a variety of precise modes of non-local signalling, such as dynamically changing according to the concentration of specific components. For the more general purposes here we subsequently restrict to the specific and analytically convenient case in which each cell creates a equivalent and fixed signalling net. Yet, even within this simplification a wide variety of distinct forms of non-local signalling can still be considered, including uniform, tip-based and polarised scenarios. A combination of linear stability analysis and numerical simulation is used to unravel the complexities of pattern formation and determine how the spatial distribution of signal through the net impacts on the pattern form.

2. Model Derivation

2.1. Collier et al model

We suppose the tissue to be formed from a set of identically-sized discrete cells, $\mathcal{C}$, arranged into either a 1-dimensional chain or 2-dimensional regular hexagonal lattice (Figure 1 (c)) and of total cell number $|\mathcal{C}|$. Each cell operates as both a *signaller* and a *receiver*, according to the activity levels of ligands and receptors at the cell membrane. Each cell is given an index r, and for two cells r and s we define their distance apart as $d_{r,s}$, measured in terms of cell diameters. For example, for a population of cells of consistent size and (approximate) diameter 10 μm, $d_{r,s} = 5$

5

would correspond to 50μm.

We base our study on the well-known Delta-Notch signalling pathway for lateral inhibition, crucial as a regulator of patterning and for the functioning of various developing and adult tissues. More precisely, we adapt the Collier *et al.* [5] model: these equations forsake detailed pathway representation for an analytically tractable two-variable model that characterises the essential elements of the process.

It is important to note that this model exhibits a number of drawbacks: from a biological perspective it does not offer the detailed molecular description consistent with our current understanding into Delta-Notch signalling, while from a patterning perspective it demonstrates a certain lack of robustness to noise. While various models have been developed to address these and other issues, we retain the original model of [5] as our "core pattern generator": given our more theoretical aims, as the prototype model it acts as a suitable reference point for comparison.

Specifically, for each cell $r \in \mathcal{C}$, we suppose receptor (U_r) and ligand (V_r) activity levels evolve according to the coupled set of equations:

$$\frac{d(U_r/U^*)}{d\tau} = F(\bar{V}_r/V^*) - \mu U_r/U^* ;$$

$$\frac{d(V_r/V^*)}{d\tau} = G(U_r/U^*) - \rho V_r/V^* .$$

Here, τ is time and U^* and V^* define typical levels of ligand and receptor activity. F and G are continuous functions $F, G : [0, \infty) \rightarrow [0, \infty)$ that describe how the activity changes according to interactions between and within cells (e.g. lateral inhibition); their specific forms are described below. μ and ρ are rate constants for the turnover of receptor and ligand. Defining $f := F/\mu$ and $g := G/\rho$ and setting $u_r = U_r/U^*$, $v_r = V_r/V^*$, $t = \mu\tau, \nu = \rho/\mu$, yields the non-dimensional system:

$$\frac{du_r}{dt} = f(\bar{v}_r) - u_r ,$$

$$\frac{dv_r}{dt} = \nu[g(u_r) - v_r] . \tag{1}$$

The function f determines the upregulation of receptor activity: this will be directly dependent on cell to cell ligand-receptor binding, and hence will vary according to the average ligand activity received by the cell from its neighbourhood, defined as $\bar{v}_r$: a standard assumption, as taken in [5] and similar models, is to assume a cell only signals to its nearest neighbours. Here we assume long range (filopodia-mediated) signalling across some non-local neighbourhood, and the variable $\bar{v}_r$ will be defined accordingly. Overall, $f : [0, \infty) \to [0, \infty)$ is set as an increasing function of $\bar{v}_r$, reflecting that high ligand activity in a cell's neighbourhood will lead to greater ligand-receptor binding and hence high receptor activity in the receiving cell.

In the lateral-inhibition interactions of Delta and Notch, high receptor activity in a cell down-regulates its ligand activity: see Figure 1 (a). Specifically, we assume $g : [0, \infty) \to [0, \infty)$ to be a continuous and decreasing function of receptor activity. Following the standard choice of Hill-type functions as taken in [5], we set

$$f(y) = \frac{y^{h_1}}{a^{h_1} + y^{h_1}}, \text{and } g(y) = \frac{b^{h_2}}{b^{h_2} + y^{h_2}}, \tag{2}$$

where $a, b > 0$ and Hill coefficients $h_1, h_2 \geq 1$.

2.2. Long range signalling

As stated, our principal aim is to investigate how non-local, direct-contact signalling can impact on tissue patterning. Specifically, we assume that each cell has a capacity to form a net of filopodial-like extensions through which ligand-receptor interactions can occur. Filopodia-mediated cell to cell signalling will undoubtedly be subject to extensive regulatory control, depending on the state of both an individual cell and its environment. For specific applications, due consideration would therefore need to be made of:

- *the physical structure of the net*, characterised by the numbers, lengths and orientations of the extensions – filopodia/cytonemes can be found to range up to 100s of microns (10s of cell lengths) and can display a distinct polarisation or orientational bias;

- *the distribution of signalling molecules throughout the net*, for example, whether they are distributed uniformly along filopodia or concentrated at apical ends,

or whether just ligand, just receptor or both components are localised to filopodia.

Aiming for a more general treatment, we condense these aspects into a single modelling term, $w(s, r; \cdot)$: a *weighting function* defining the level of signalling from a signaller cell $s \in \mathcal{C}$ to a receiver cell $r \in \mathcal{C}$. We note that $0 \leq w(s, r; \cdot) \leq 1$. This function could potentially depend on several factors, including: the signalling activity of the signaller or receiver – high/low activity in either the signalling or receiving cell could promote or inhibit the formation of long-range contacts; environmental factors, such as extracellular chemical signalling molecules.

For a cell j we can therefore define a *signalling neighbourhood* (see Figure 2 (a)),

$$\mathcal{S}_j = \{r : r \in \mathcal{C} \text{ and } w(j, r; \cdot) > 0\} \,,$$

and a *receiving neighbourhood* (see Figure 2 (b)),

$$\mathcal{R}_j = \{s : s \in \mathcal{C} \text{ and } w(s, j; \cdot) > 0\} \,.$$

The former defines the set of cells that receive signal from cell j, while the latter defines the set of cells from which it receives signal. The sizes of these neighbourhoods will be limited by the maximum lengths of filopodia and are not necessarily the same: for example, one cell may exclusively signal to its nearest neighbours, but receive signals from distant cells via their extension of ligand-laden filopodia.

Through the above we define $\bar{v}_r$ for model (1). Specifically, we assume that at time t the cell r receives the weighted proportion $w(s, r; \cdot)l_s(t)$ of ligand from the signaller at s. Hence, the total amount received will be given by

$$\bar{v}_r(t) = \sum_{s \in \mathcal{R}_r} w(s, r; \cdot)l_s(t) \,. \tag{3}$$

Any cell only has a finite amount of active ligand to distribute at any given timepoint: here we assume that the full activity is distributed[1], resulting in the conservation

---

[1]For example, cells have an abundance of free receptors that allows ligand to be more or less instantaneously bound.
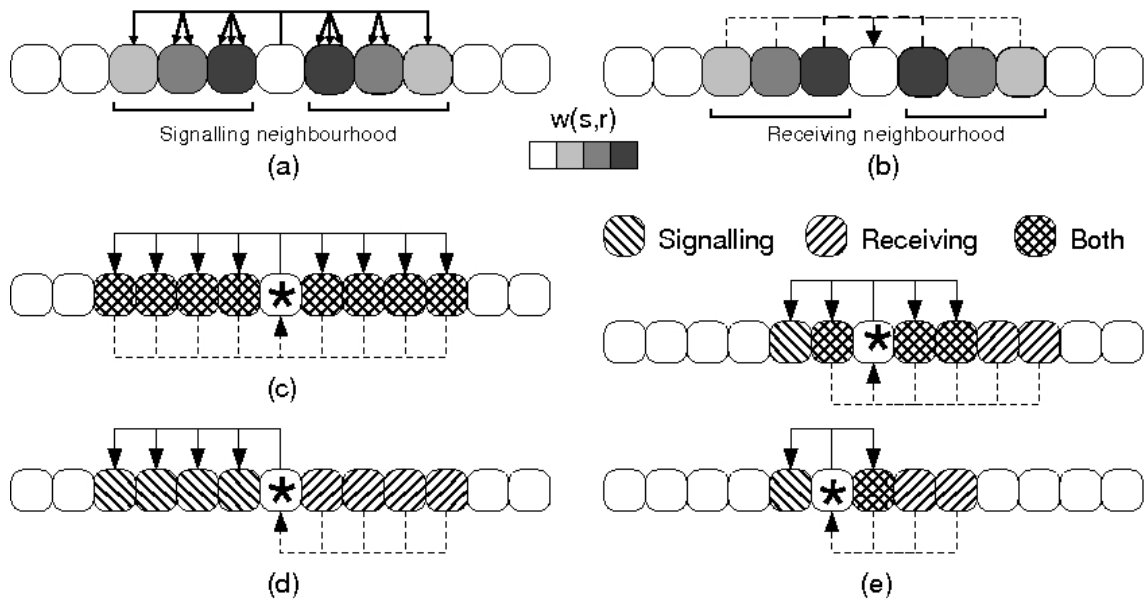
Figure 2: Signalling and receiving neighbourhoods. (a) Each cell signals to other cells in a non-local signalling neighbourhood, with the amount signalled varying with signaller/receiver positions: as an example, here the closest cells receive the greater share and distant cells little or none. (b) Each cell receives signals from other cells in its receiving neighbourhood, with the sum total providing the input for upregulation of receptor activity. (c-e) Illustrations showing potential signalling/receiving neighbourhoods for different scenarios: see text for explanation.

law

$$\sum_{r \in \mathcal{S}_s} w(s, r; \cdot) = 1 \,. \tag{4}$$

Of course, in the event that full ligand activity is not transferred, w is still constrained such that $\sum_{r \in \mathcal{S}_s} w(s, r; \cdot) \leq 1$. However, potential cell-cell variations between signalling distributions would not lead to a similar law for reception: a cell r could receive either a larger ($\sum_{s \in \mathcal{R}_r} w(s, r) > 1$) or smaller ($\sum_{s \in \mathcal{R}_r} w(s, r) < 1$) share according to the ligand distribution of surrounding cells.

Non-local signalling nets will be described via the following terminologies:

- *Fixed or dynamic.* Fixed nets are assumed to be time-independent, i.e. the weighting function $w(s, r)$ does not depend on t and neighbourhoods are fixed throughout the patterning process. Dynamic nets refers to cases where w may vary in time (for example, with the concentration of ligand/receptor activities).

- *Homogeneous or heterogeneous.* For homogeneous we assume every cell generates an equivalent signalling net: hence, $w(s_1, r_1) = w(s_2, r_2)$ where the positional relationships between s_1 and r_1 and between s_2 and r_2 are equivalent. In heterogeneous cases, the arrangements vary from cell to cell.

- *(Radially) symmetric or asymmetric.* For (radially) symmetric nets we suppose the weighting function is radially symmetric about the signalling cell: $w(s, r_1) = w(s, r_2)$ if $d_{s,r_1} = d_{s,r_2}$ for two receiving cells r_1 and r_2. Asymmetric cases do not display such properties, but could include polarised/oriented scenarios, where signalling is focussed into one or more direction.

Figure 2 (c-e) shows some examples of these in a one-dimensional chain. In (c) we consider fixed, homogeneous and symmetric nets where each cell signals to the four neighbours either side (although the proportion received may still vary with distance from the signaller): in this case, a cell's signalling and receiving neighbourhoods will be identical. In (d) we consider a fixed, homogeneous and asymmetric net where ligand is only transferred leftwards: signalling/receiving neighbourhoods are distinct, but of equal size. In (e) we illustrate two adjacent cells in a population with fixed, heterogeneous nets: each cell's signalling/receiving neighbourhood can

be of distinct size and shape.

To illustrate, we consider appropriate weighting functions for some basic examples as follows.

- In an *autocrine* signalling system each cell signals only to itself: e.g. ligand binds to receptor on the same cell. Hence, we would set

$$w(s, r) = \begin{cases} 1 & \text{if } d_{s,r} = 0 \\ 0 & \text{otherwise} \end{cases}.$$

  Receiving and signalling neighbourhoods become the single element sets composed of the cell itself. In the context of the Delta-Notch model, we have $\bar{v}_r(t) = v_r(t)$ and the $|\mathcal{C}| \times 2$ order system 1 reduces into $|\mathcal{C}|$ decoupled second-order systems.

- In *nearest-neighbour juxtacrine* signalling we assume a cell shares its ligand equally across its nearest neighbours. Specifying the exact weighting function depends on the precise geometry: for the regular arrangements of Figure 1 (c) we would have

$$w(s, r) = \begin{cases} 1/N & \text{if } d_{s,r} = 1 \\ 0 & \text{otherwise} \end{cases},$$

  where $N = 2$ (for the 1D chain) or $N = 6$ (for the 2D hexagonal array). This case recapitulates the form used in the Collier *et al* model ([5]) for lateral inhibition.

3. Fixed and homogeneous signalling nets

For the more general aims here, we employ the remainder of the paper to focus on the analytically convenient case where signalling nets are fixed and homogeneous. We do permit variation from symmetric to asymmetric forms to determine how the precise spatial distribution of signal through the net impacts on patterning.

Given that direct contact is required, signalling will be restricted by the maximum reach of filopodia. We therefore parametrise the model in terms of the *signalling range R*, defined in terms of cell diameters and marking the distance between the

signalling cell and the most distant receiving cell[2]: we therefore have $w(s, r) = 0$ for $d_{s,r} > R$. Note that we will exclude any possibility of autocrine signalling by setting $w(r, r) = 0$.

3.1. Weighting functions

3.1.1. One-dimensional chain

In the one-dimensional case we let each cell's index define its position along the chain. For a receiver at r and a signaller at $s = r + n$ (for $n \in \mathbb{Z}$) we consider the weighting function

$$w(r+n, r) = \begin{cases} w^* \gamma_1 e^{-\sigma_1 (n+\mu_1)^2} & \text{if } -R \le n < 0 \\ w^* \gamma_2 e^{-\sigma_2 (n-\mu_2)^2} & \text{if } 0 < n \le R \\ 0 & \text{otherwise} \end{cases} . \tag{5}$$

In the above, $\sigma_{1,2}, \mu_{1,2}$ and $\gamma_{1,2}$ are constant parameters that define the functional shape, while w^* is the appropriate normalising constant that ensures (4).

The above weighting function can encompass a broad range of signalling classes, as we illustrate in Figure 3. We can include both symmetric (top row) and asymmetric (bottom row) signalling scenarios. Figure 3 (a) considers a "diminishing" form in which signalling is concentrated to the nearest cells and decreases as the distance from signaller to receiver increases. Figure 3 (c) illustrates a "targeted" form, where ligand is predominantly passed to cells located more than one cell diameter away. Polarised equivalents are illustrated in Figure 3 (b) and (d). For purposes of analysis, we also consider the following special limiting cases.

- *Symmetric (polarised) uniform signalling, SU (PU). We set $\gamma_1 = 1$ ($\gamma_1 = 0$),*

---

[2]Hypothetically, ligand attached to the apical tip of one filopodium could contact a receptor on the apical tip of another: consequently, this range could potentially be up to twice the maximum filopodium length.
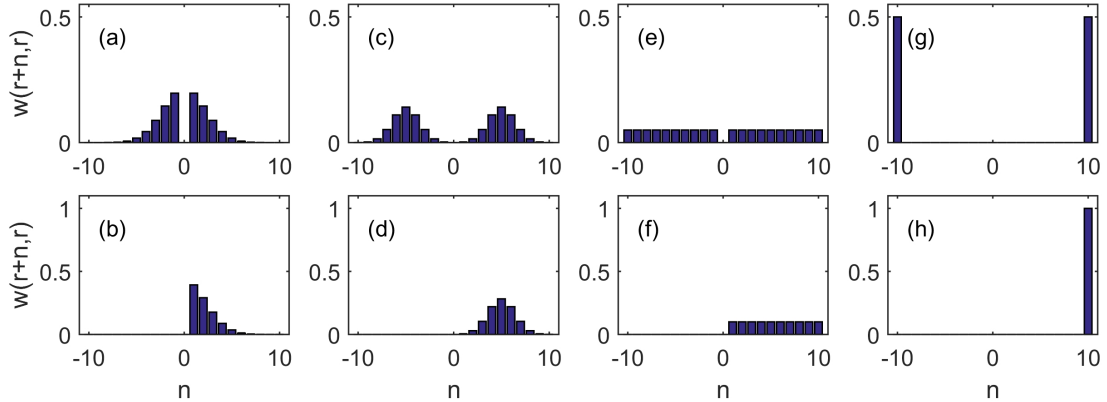
Figure 3: Examples of weighting function (5): (a-b) Symmetric/polarised distributions in which cells closest to the source cell at 0 receive the greatest proportion of signal; (c-d) Symmetric/polarised distributions in which signal is targetted to more distant cells. (e-f) Symmetric/polarised uniform signalling. (g-h) Symmetric/polarised distal signalling. For all forms we set $R = 10$, $\gamma_{1,2} = 1$ for symmetric ($\gamma_1 = 0, \gamma_2 = 1$ for polarised) signalling, and: (a-b) $\sigma_{1,2} = 0.1$, $\mu_{1,2} = 0$; (c-d) $\sigma_{1,2} = 0.25$, $\mu_{1,2} = 5$; (e-f) $\sigma_{1,2} = \mu_{1,2} = 0$; (g-h) $\sigma_{1,2} = \infty$, $\mu_{1,2} = 10$.

$\gamma_2 = 1$, $\mu_{1,2} = \sigma_{1,2} = 0$. Hence (5) becomes (Figure 3 (e-f)):

$$(\text{SU}) \qquad w(r + n, r) = \begin{cases} \frac{1}{2R} & \text{if } 0 < |n| \leq R \\ 0 & \text{otherwise} \end{cases} \quad ;$$

$$(\text{PU}) \qquad w(r + n, r) = \begin{cases} \frac{1}{R} & \text{if } 0 < n \leq R \\ 0 & \text{otherwise} \end{cases} \quad .$$

- *Symmetric (polarised) distal signalling, SD (PD).* We set $\gamma_1 = 1$ ($\gamma_1 = 0$), $\gamma_2 = 1$, $\mu_{1,2} = R$ and $\sigma_{1,2} \to \infty$. Hence (5) becomes (Figure 3 (g-h)):

$$(\text{SD}) \qquad w_{r+n,r} = \begin{cases} 1/2 & \text{if } |n| = R \\ 0 & \text{otherwise} \end{cases} \quad ;$$

$$(\text{PD}) \qquad w_{r+n,r} = \begin{cases} 1 & \text{if } n = R \\ 0 & \text{otherwise} \end{cases} \quad .$$

3.1.2. Two-dimensional array

We consider the regular hexagonal lattice (see Figure 1 (c)) and weighting function:

$$w(s,r) = \begin{cases} w^* e^{-\sigma_1 (d_{s,r} - \rho)^2} e^{\sigma_2 \cos(\alpha(\theta_{s,r} - \phi))} & \text{if } 0 < d_{s,r} \leq R \\ 0 & \text{otherwise} \end{cases}. \tag{6}$$

In the above, $\theta_{s,r} \in (-\pi, \pi]$ defines the angular bearing between the signalling and receiving cells. $\sigma_{1,2}, \rho, \phi$ and α are parameters that control the shape and form of the weighting function, while w^* is the normalising coefficient.

As in 1D, equation (6) can be tailored to create a variety of distinctive signalling nets:

- *Radially symmetric signalling.* Setting $\sigma_2 = 0$ imposes radial symmetry: figure 4 (a-c) plots examples for (a) uniform symmetric signalling, (b) locally targetted symmetric signalling, and (c) distally targetted symmetric signalling.

- *Axial signalling.* Polarity-inducing cues may allow filopodia to become oriented along a particular axial direction: these scenarios can be reproduced by setting $\sigma_2 > 0$ and $\alpha = 2$. Figures 4 (d)-(e) illustrate axial signalling examples where all cells, (d), or a subset of cells, (e), along a particular axis are signalled.

- *Polarised signalling.* Signalling may also be concentrated along a unique direction. Setting $\sigma_2 > 0$ and $\alpha = 1$ generates polarised signalling, for example see Figure 4 (f).

3.2. Linear stability analysis

To investigate the possibility of pattern formation we perform a linear stability analysis under certain idealised scenarios. Note that such analyses have previously been performed for the nearest-neighbour juxtacrine signalling of [5]: here, we extend that analysis to investigate how patterning will be altered in systems capable of non-local, direct-contact signalling. For simplicity we concentrate on the 1D sce-
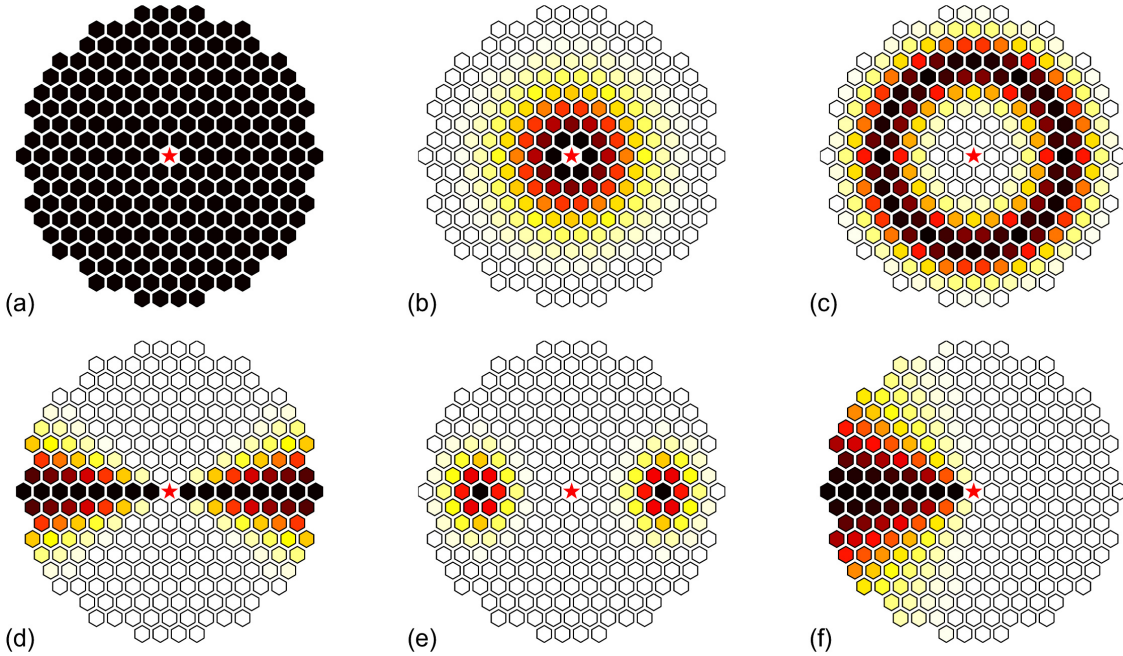
Figure 4: Illustrations of the two-dimensional weighting function (6), where the weighting function (white=low, dark=high) is indicated by the colorscale. (a-c) Radially symmetric signalling; (d-e) Axial signalling; (f) Polarised signalling. For all plots we set $R = 8$ and (a) $\sigma_1 = \rho = \sigma_2 = \alpha = \phi = 0$; (b) $\sigma_1 = 0.1$, $\rho = \sigma_2 = \alpha = \phi = 0$; (c) $\sigma_1 = 0.5, \rho = 5$, $\sigma_2 = \alpha = \phi = 0$; (d) $\sigma_1 = \rho = 0$ $\sigma_2 = 5, \alpha = 2, \phi = 0$; (e) $\sigma_1 = 0.5, \rho = 5$ $\sigma_2 = 5, \alpha = 2, \phi = 0$; (f) $\sigma_1 = \rho = 0$ $\sigma_2 = 5, \alpha = 1, \phi = 0$.

nario[3] outlined in section 3.1, assuming that cells form an infinite chain. The linear stability analysis itself closely follows that outlined in [5].

We first note that the system (1) possesses a single positive homogeneous steady state (u_0, v_0): a state in which Notch/Delta activity levels are the same across the cellular field. Note that at the steady state we have $f(g(u_0)) = u_0$, $v_0 = g(u_0)$, with its uniqueness stemming from $f(g(u))$ being monotonically decreasing for all $u \geq 0$. To examine stability, we set $\hat{u}_r = u_r + u_0$ and $\hat{v}_r = v_r + g(u_0)$, where the new variables track disturbances from the steady state. Substituting into (1) and

---

[3]The extension to higher dimensions is straightforward and does not significantly change the principal message here: the most notable difference is more stringent requirements on the feedback strength, as the signal must be distributed over a larger number of cells, see [5] for details.

ignoring nonlinear terms (and dropping the "hats" for notational simplicity), we obtain the linearised system

$$
\begin{aligned}
\dot{u}_r &= A\bar{v}_r - u_r, \\
\dot{v}_r &= \nu B u_r - \nu v_r,
\end{aligned}
\tag{7}
$$

where u_r, v_r denote the new variables, and "$\cdot$" indicates the time derivative. Note that in the above we have set $A := f'(g(u_0))$ and $B := g'(u_0)$.

Following a standard stability analysis, for example see [15], we look for solutions of the form $u_r, v_r \sim e^{\lambda t + ikj}$, where λ is the (temporal) eigenvalue. k defines the (discrete) wavenumber: solutions for $k > 0$ correspond to patterned solutions with corresponding pattern wavelength $2\pi/k$. Substituting into (7) and simplifying yields the dispersion relation

$$
\lambda^2 + (1 + \nu)\lambda + \nu(1 - ABK(k)) = 0 \,,
\tag{8}
$$

where the function $K(k)$ differs according to the averaging term/weighting function. Patterns are expected to emerge from perturbations of the uniform solution only if there exists a non-empty set of discrete values of the form $k = 2\pi/m$, $m = 2, 3, 4\ldots$ for which $\max(\mathrm{Re}(\lambda)) > 0$. This requirement for such discrete k results from the discrete nature of the cellular field: only discrete wavelengths corresponding to $2, 3, 4, \ldots$ cell diameters are relevant for patterning.

For the one-dimensional scenario considered in section 3.1 we have

$$
K(k) = \sum_{n=-R, n\neq 0}^{R} w(r + n, r)\left(\cos(nk) + i\sin(nk)\right)
\tag{9}
$$

In particular, for symmetric signalling scenarios ($w(r - n, r) = w(r + n, r)$) the imaginary component disappears and we obtain

$$
K(k) = 2\sum_{n=1}^{R} w(r + n, r)\cos(nk) \,.
\tag{10}
$$

In this case, patterned solutions are expected to form provided

$$
AB < \frac{1}{K_{min}} \,,
\tag{11}
$$

16

where $K_{min} < 0$ denotes the minimum of the real function $K(k)$ for $k \in [0, \pi]$. Noting that A and B define the slopes of the feedback functions f and g at the homogeneous steady state and defining the magnitude $|AB|$ as the feedback strength, condition (11) stipulates that the feedbacks must operate in opposing fashion (as for a lateral inhibition mechanism), and that the feedback strength must be sufficiently high for patterns to emerge, $|AB| > |1/K_{min}|$.

A detailed analysis for the general weighting function (5) is not particularly illuminating due to its large number of free parameters. Instead, we focus on the two idealised scenarios of uniform and distal signalling: each corresponds to a specific limit of (5) and can therefore provide an indication of behaviour for more general forms.

3.2.1. Uniform signalling

We consider the uniform signalling scenarios (SU) and (PU). Here, we obtain

$$
\begin{aligned}
K_{SU}(k) &= \frac{(\sin((R+1/2)k) - \sin(k/2))}{2R\sin(k/2)}, \\
K_{PU}(k) &= \frac{((\sin((R+1/2)k) - \sin(k/2)) + i\,(\cos((R+1/2)k) - \cos(k/2)))}{2R\sin(k/2)},
\end{aligned}
$$

where we have employed Lagrange's trigonometric identities. Note that for $R = 1$ we simply have $K(k) = \cos k$ for symmetric signalling and $K(k) = \cos k + i \sin k$ for polarised signalling. In either case, the condition for patterning simplifies to $AB < -1$: for the symmetric scenario, this case exactly recapitulates that of [5].

Figure 5 (a) plots the relationship between the required feedback strength and the signalling range for instability of the uniform solution to occur under symmetric uniform signalling. First, we note that larger R require larger $|AB|$: intuitively, as the number of cells within signalling range increases, the activating ligand is shared across a wider field and stronger feedback is necessary to generate patterning.

However, rather than a simple linear dependency, Figure 5(a) suggests that the feedback strength saturates for larger values of R. A combination of numerical investigations and algebra suggests that as R increases, the minimum of $K_{SU}(k)$
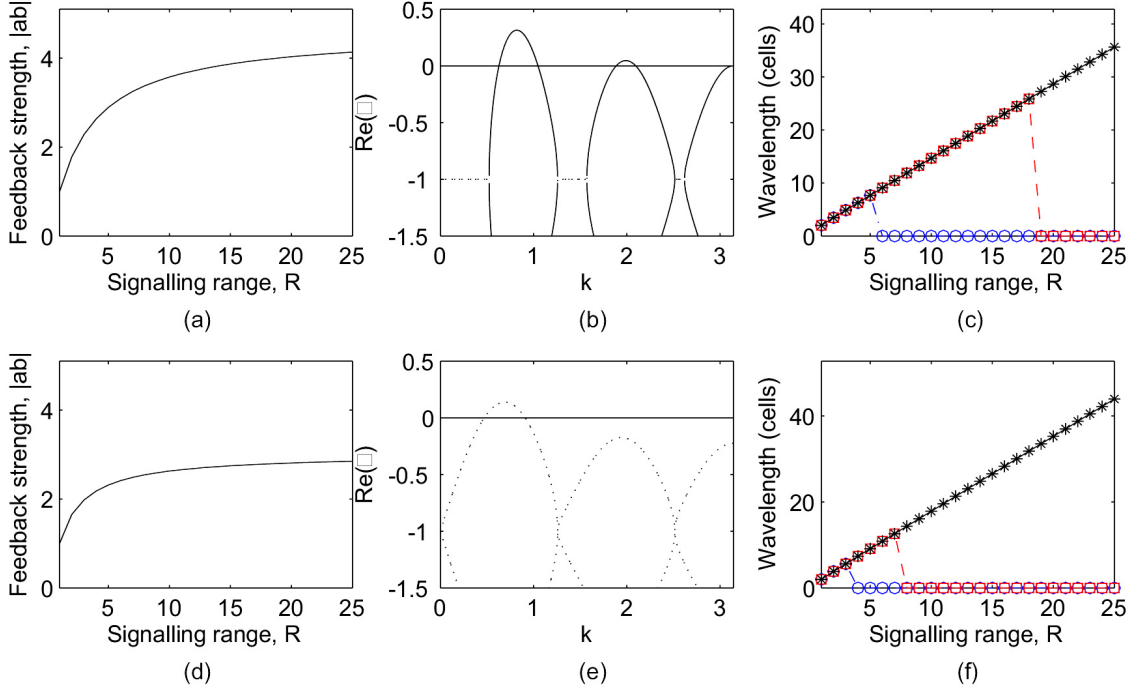
17

Figure 5: Top row: Linear stability analysis for symmetric uniform signalling. (a) Critical value of $|AB|$ needed for pattern formation as a function of the signalling range R; (b) Typical dispersion relation, plotting $\text{Re}(\lambda)$ as a function of the wavenumber (k). Purely real eigenvalues are indicated by solid lines; complex eigenvalues denoted by dotted lines. Here, $|AB| = 5$ and $R = 5$, resulting in multiple ranges of unstable wavenumbers. (c) Plot of the fastest growing wavelength as a function of signalling range for (solid-black-stars) $|AB| = 5$, (dashed-red-squares) $|AB| = 4$, and (dot-dash-blue-circles) $|AB| = 3$. Bottom row: Linear stability analysis for polarised uniform signalling. (d) Critical value of $|AB|$ needed for pattern formation as a function of signalling range R; (e) A typical dispersion relation: here $|AB| = 4$ and $R = 5$. (f) Fastest growing wavelength as a function of R for (solid-black-stars) $|AB| = 4$, (dashed-red-squares) $|AB| = 3$, and (dot-dash-blue-circles) $|AB| = 2$.

converges to $\sin x^* / x^*$ at corresponding wavenumber x^*/R, where x^* is given by the solution to $\tan x^* = x^*$ ($x^* = 4.493409\ldots$). Subsequently, from (11) we have an upper limit on the necessary $|AB|$: for sufficiently strong feedback in the underlying signalling network, i.e. $|AB| \gtrsim 4.6$, the instability condition is satisfied regardless of R and there is no upper limit on the signalling range for pattern formation to occur.

18

Note further that for the functions f and g given in equation (2), feedback will be controlled by parameters a, b, h_1, and h_2. A reasonably straightforward calculation (see Appendix) determines $|AB| < h_1 h_2$. Taken with the observations above, for functional forms (2) and arbitrarily large R, a *minimum* for the Hill function coefficients will therefore be $h_1 h_2 \gtrsim 4.6$.

We next explore expected pattern wavelengths. Examining K_{SU} we observe that $K(k) < 0$ for $\sin((R + 1/2)k) < \sin(k/2)$: hence, we can expect multiple ranges of unstable wavenumbers in $[0, \pi]$, from short (wavelengths of 2 cells) to much longer wavelengths. Figure 5 (b) plots a representative dispersion relation in the unstable regime, showing these multiple ranges. We define the *expected wavelength* via the wavenumber that maximises $\text{Re}(\lambda)$: wavelengths close to this value will grow the quickest, at least initially and under random initial perturbations, and therefore it offers an insight into the nonlinear pattern wavelength.

In Figure 5 (c) we plot the expected pattern wavelength (in terms of cell diameters) as a function of R under various feedback strengths: in each case we observe an identical quasi-linear increase in the expected wavelength, suggesting that the spacing in emerging patterns is relatively robust to kinetic parameters but crucially dependent on the signalling range. For lower feedback strengths the expected wavelength can collapse to zero above a critical R, if we cross the instability/stability boundary shown in Figure 5 (a); note that for the choice $|AB| = 5$ this will never happen and we expect indefinite increase of the expected wavelength with R.

Figure 5 (d-f) summarise the results of an equivalent analysis under polarised uniform signalling. The overall trends are consistent, although two distinct aspects are noted. First, we observe an expanded instability regime, in that patterning can occur at a lower feedback strength for equivalent R, Figure 5 (d): intuitively, for polarised signalling the ligand is shared across half the number of cells and the required feedback to trigger patterning is lower. Second, the imaginary component to $K_{PU}(k)$ ensures complex eigenvalues for all wavenumbers, see Figure 5 (e). Consequently we can expect that *emerging* solutions will oscillate in both space and time, raising the potential for long-term nonstationary and patterned solutions.

19

3.2.2. Distal signalling

For the distal signalling scenarios (SD) and (PD) we have

$$K_{SD}(k) = \cos Rk\,,$$
$$K_{PD}(k) = \cos Rk + i \sin Rk\,.$$

As for uniform signalling, we immediately note that the polarised case generates complex eigenvalues and, hence, oscillating solutions.

For either symmetric or polarised distal signalling the condition for patterning simplifies to $AB < -1$: the capacity to pattern is independent of the signalling range and rests solely on the underlying signalling interactions (represented via the functional forms f and g). However, R may still impact on the form of patterns via their expected wavelength. Here we find that at large R multiple unstable wavenumbers grow at an identical rate: for example, for $R = 4$ each of the 2-, 4- and 8-cell wavelengths are predicted to grow equally fast. Consequently, the linear stability analysis is inconclusive regarding the predicted wavelength.

4. Numerical Simulations

To gain further insight we perform a numerical analysis. Our focus remains on the spatial distribution of signal through the signalling net and we continue to adopt the 1D and 2D weighting functions introduced above. For R we assume it spans a range from a single cell (i.e. only nearest-neighbours are signalled) to $O(10)$ cell lengths: filopodia/cytoneme lengths have been reported of up to 100s of microns [24], corresponding to 10s of cell lengths based on an average cell diameter of 10 μm.

Kinetic term parameters are simply fixed at values that ensure any linear instability condition is met for the given weighting function. Note that we exclusively consider $\nu = 1$: the choice $\nu \neq 1$ does not significantly alter the pattern, but does impact on the patterning timescale.

4.1. One-dimensional cell chain

4.1.1. Symmetric signalling

We first consider a one-dimensional cell chain and exploit the convenient forms of uniform/distal signalling to investigate pattern variation as the range is altered. To minimise any impact from boundaries we impose periodic boundary conditions: the "first" and "last" cells are considered adjacent, so that the chain ends join to form a cellular ring. Initially, ligand and receptor activity levels are given a small, spatially random perturbation from the uniform steady state distribution.

Figure 6 demonstrates the output from representative simulations under symmetric uniform (SU) and distal (SD) signalling, as R is increased. Solutions are computed in each case until a (numerical) steady-state solution is obtained, i.e. such that there is no perceptible change to the solution; theoretically, the solution could simply represent a long-lived transient, yet given the finite time scales of embryonic developmental processes, any such transient can be considered a final solution. For descriptive purposes we assume a cell adopts a "primary fate" when receptor levels are low and ligand levels are high, and a "secondary fate" otherwise, consistent with SOP specification during *Drosophila* bristle patterning.

Figure 6(a) illustrates the simulation results for uniform signalling. Clearly, and in line with the earlier analysis, a lengthening of the pattern wavelength is observed as the filopodial range increases. Specifically, we find an emerging pattern in which isolated cells adopt a primary fate, interspersed with an R-dependent region of secondary fate cells. In the lateral-inhibition mechanism, primary fate adoption will suppress similar behaviour in neighbouring cells: here, this suppression spreads through the signalling neighbourhood and a sparse pattern results. We note that when emerging from random initial conditions, pattern wavelengths are consistent with the expected wavelength: it is possible to "force" the pattern into other wavelengths by biasing the initial conditions appropriately.

Simulations for an equivalent analysis under distal signalling are depicted in Figure 6 (b). The earlier analysis was less revealing on how pattern depends with R: this unpredictability transfers to numerical solutions where, for larger R, we observe a
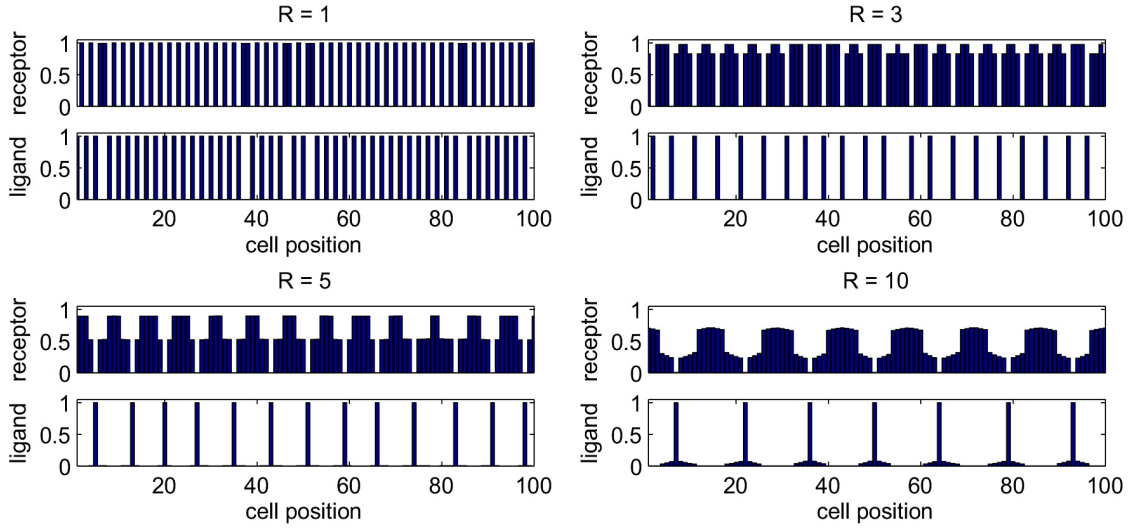
(a) Uniform signalling
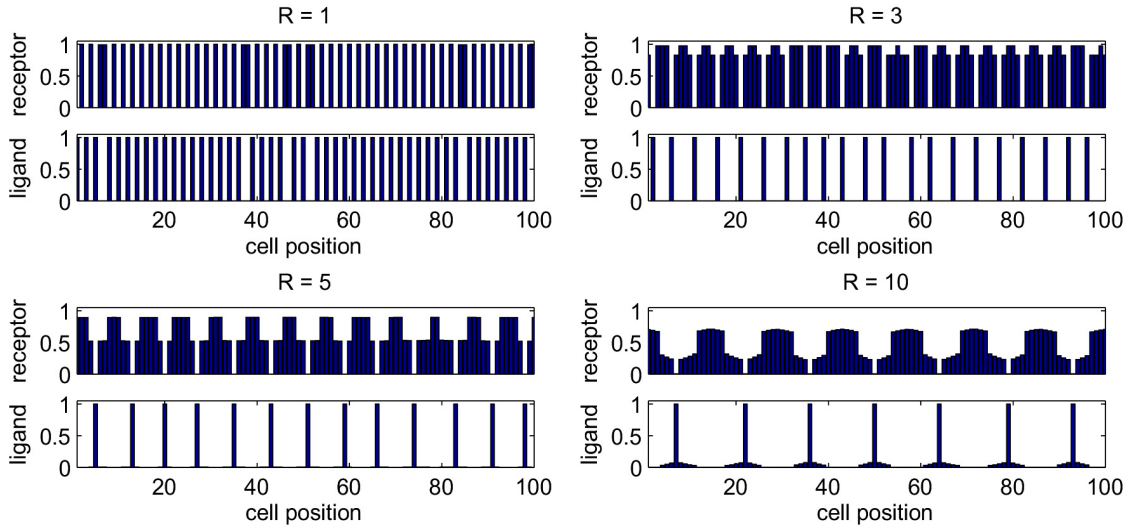
(b) Distal signalling

Figure 6: Numerical solutions of model (1) with (3,5) and under (SU) or (SD) signalling. (a) SU signalling for distinct R, as specified above each plot. Increasing R expands the pattern wavelength to create a single primary fate cell (high ligand/low receptor) in an expanding block of secondary fate cells (low ligand/high receptor). (b) SD signalling for distinct R. "Mixed-mode" patterns are observed composed of single and multi-cell blocks of primary fate cells are interspersed with secondary cells. For these simulations we set: (a) $\nu = 1$, $a = b = 0.1$, $h_1 = h_2 = 3$ and SU signalling; (b) $\nu = 1$, $a = b = 0.1$, $h_1 = h_2 = 2$ and SD signalling. Simulations are computed for a chain of 100 cells until a numerical steady state is reached. Numerical computations invoke the ode15s routine in Matlab.

tendency towards "mixed mode" patterns in which both short (alternating cell fate) and long-wavelength patterns can emerge in distinct regions of the field. In contrast to uniform signalling we now frequently observe "block patterning", where blocks of adjacent cells adopt the primary cell fate. From an intuitive perspective, the lack of direct signalling into the adjacent cells (unless $R = 1$) prevents a primary fate cell from suppressing similar activity in its closest neighbours.

Uniform and distal signalling are analytically convenient, yet in practice we would expect signalling to vary with the distribution of filopodial lengths and directions, along with the mode of ligand distribution. We therefore extend our study to determine whether similar patterning occurs under more smoothly distributed weighting functions: naturally, we would expect ligand distribution to steadily diminish at large distances between signal and receiver, for example due to fewer longer filopodia and the decreased likelihood of forming a contact.

We first suppose the weighting function decreases monotonically from the signalling cell outwards, varying $\sigma_{l,r}$ in (5) to control the extent to which more distant cells receive signal: see Figure 7 (a-c, top row) for the weighting function distributions. Simulations indicate patterning similar to the uniform signalling case considered above: an isolated primary fate cell emerges within a region of secondary fate cells, where the region of secondary fate cells increases as more signal is shifted to the more distant cells.

Next, weighting functions are changed so that the focal point of signalling shifts from closer to more distant cells: specifically, we vary $\mu_{l,r}$ in (5) while keeping other parameters fixed, Figure 7 (d-f, top row). The corresponding patterns are somewhat similar to the distal signalling case, but are considerably more regular: we obtain regularly spaced and sized blocks of primary fate cells, separated by similar blocks of secondary fate cells.

4.1.2. Polarised signalling

We extend our simulations to examine the impact of polarised signalling where, for a one-dimensional chain, ligand is distributed asymmetrically about its centre. Note
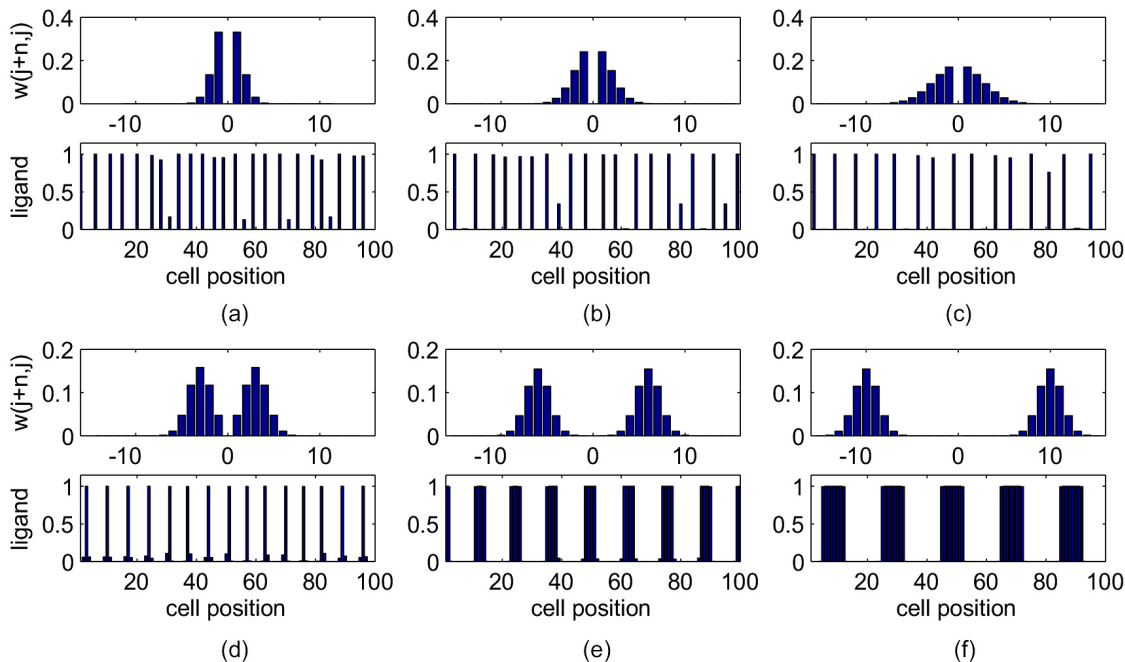
Figure 7: Numerical solutions of (1,3,5) for more general weighting functions. (a-c) Signalling decreases with distance between receiving and signalling cells: allowing distant cells to receive more signal results in a sparser pattern of primary fate cells. We take (5) with $\gamma_1 = \gamma_r = 1$, $\mu_l = \mu_r = 0$ and (a) $\sigma_l = \sigma_r = 0.3$, (b) $\sigma_l = \sigma_r = 0.15$, (c) $\sigma_l = \sigma_r = 0.075$. (d-f) Concentrated signalling is steadily shifted from nearer to more distant cells: the resulting pattern is formed of alternating blocks of primary and secondary fate cells. We take (5) with $\gamma_1 = \gamma_r = 1$, $\sigma_l = \sigma_r = 0.3$ and (d) $\mu_l = \mu_r = 3$; (e) $\mu_l = \mu_r = 0.6$, (f) $\mu_l = \mu_r = 10$. Note that for all simulations we set $\nu = 1$, $a = b = 0.1$, $h_1 = h_2 = 3$ on a ring of 100 cells.

that given the homogeneous tissue scenario, the polarity is assumed to be identical across the field: for example, all cells signal "to the left". Effectively, this assumes that some global signalling cue, such as a diffuse morphogen gradient, orients the tissue into a common polarity.

Our earlier analysis indicated that complex eigenvalues arise under polarised signalling, implying temporal oscillations during the initial pattern development. To examine how polarised signalling impacts over longer times, we consider spatio-temporal patterning as we steadily shift between completely symmetric and completely polarised signalling. Figure 8 shows the results of simulations for weighting functions that (a-d) monotonically decrease, or (e-h) are focussed at specific distance

from the signalling cell. Polarised signalling can clearly introduce spatio-temporal behaviour, such that the position of primary-fate precursor cells (isolated or in blocks) shifts along the chain. Note that the direction of the shift changes according to the direction of polarity.
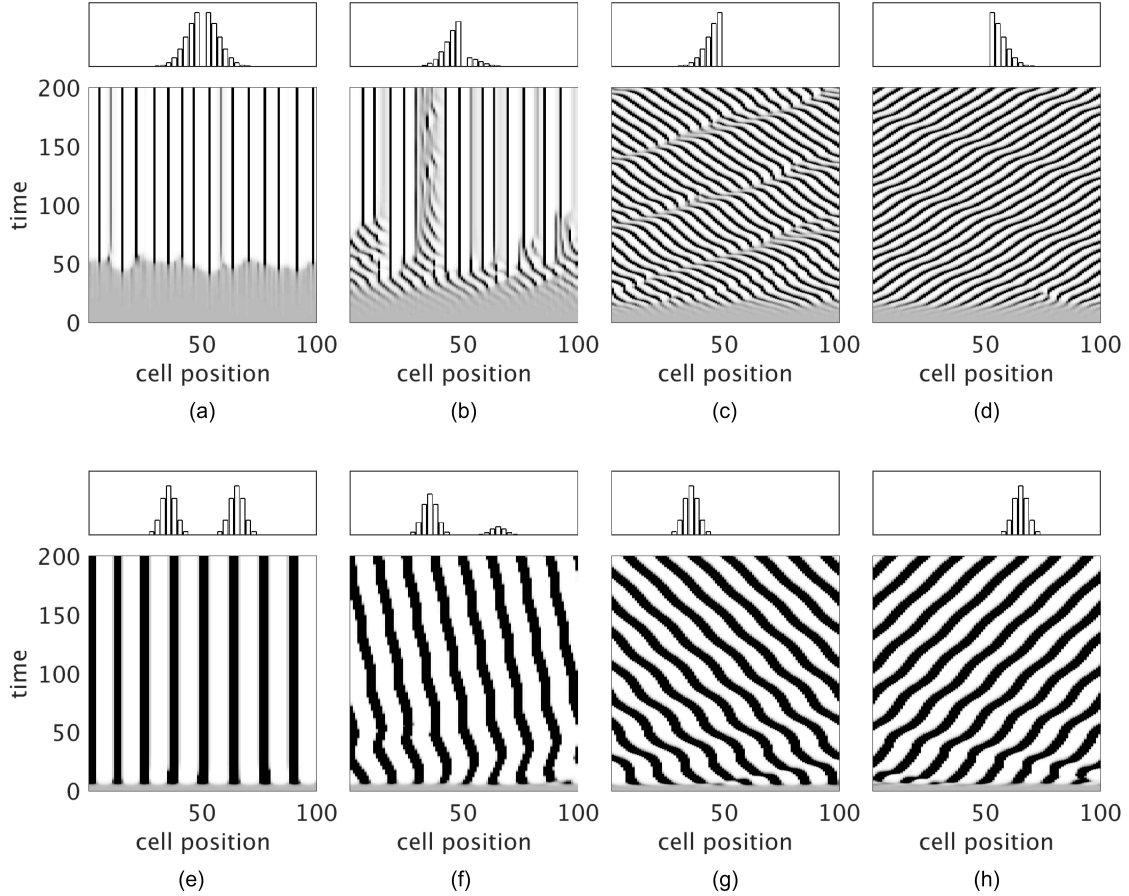

Figure 8: Spatio-temporal patterning under various forms of polarised signalling. In each frame (a-h) we plot (top) the form of the weighting function and (bottom) the positional-temporal concentration of ligand as a density plot (white = low concentration, black = high concentration). (a-d) For these simulations we take (5) with $\mu_l = \mu_r = 0$, $\sigma_l = \sigma_r = 0.075$, and: (a) $\gamma_l = \gamma_r = 1$; (b) $\gamma_l = 1, \gamma_r = 0.2$; (c) $\gamma_l = 1, \gamma_r = 0$; (d) $\gamma_l = 0, \gamma_r = 1$. (e-h) For these simulations we take (5) with $\mu_l = \mu_r = 6$, $\sigma_l = \sigma_r = 0.3$, and: (a) $\gamma_l = \gamma_r = 1$; (b) $\gamma_l = 1, \gamma_r = 0.2$; (c) $\gamma_l = 1, \gamma_r = 0$; (d) $\gamma_l = 0, \gamma_r = 1$. In all simulations we set $\nu = 1$, $a = b = 0.1$, $h_1 = h_2 = 3$ and simulations are solved on a chain of 100 cells with periodic boundary conditions.

25

4.2. Two-dimensional arrays

We extend the numerical investigation to a two-dimensional cellular field, such that cells are positioned on a hexagonal array as in Figure 1 (a). Note that for these simulations the cellular field is self-enclosed, in that cells only signal to or receive signals from others within the field: hence, cells located along or near the field edges distribute their ligand across a smaller set of cells. As for the one-dimensional case, our focus is on the signalling range and arrangement of the network and we consider fixed and homogeneous scenarios. We take the two dimensional weighting function (6) under various signalling forms, as discussed in Section 3.1.2.

4.2.1. Radially symmetric signalling

We first consider uniform and radially symmetric about the signalling cell (see Figure 4 (a)), exploring how pattern formation changes as the size of the signalling region is altered. Simulations plotted in Figure 9 (a-c) show representative patterns as we expand the signalling range: as in the 1D case we observe isolated cells that adopt the primary fate, surrounded by a field of secondary fate cells that grows with the signalling range. This behaviour is consistent with experimental observations in [7]: disrupting filopodia formation during *Drosophila* SOP specification leads to their overproduction and decreased spacing. Here, disrupting filopodia formation is equivalent to a contraction in the signalling range and we generate a greater number of primary fate cells.

We next consider a radially symmetric scenario in which signalling is concentrated into specific cells located some target distance away, see Figure 4 (b-c). Figure 9 (d-f) plots simulation results as the target distance between signalling and receiving cells changes. Consistent with earlier simulations of the equivalent one-dimensional scenario, as we move the target distance further from the signalling cell we shift to a pattern of "block" patterning: patches of primary fate cells in a field of secondary fate cells.
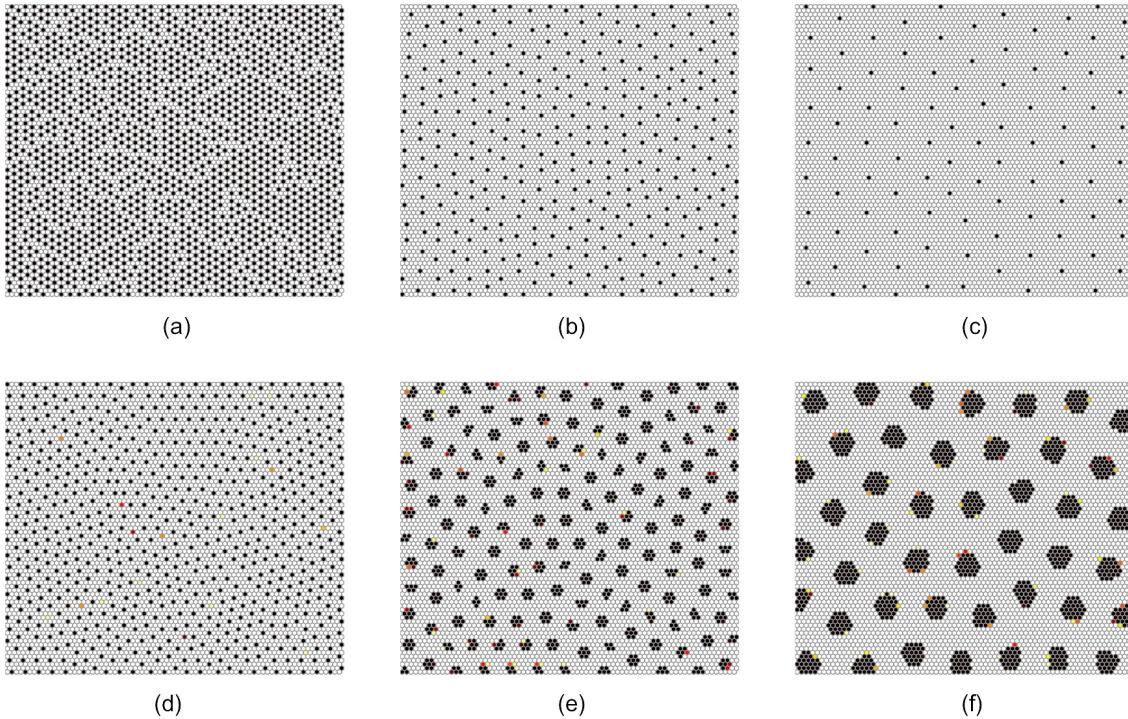
Figure 9: Pattern formation in regular hexagonal cells arrays and radially symmetric signalling. For each simulation we solve (1) under a weighting function of the form (6). Each cell is represented by its activity, with black indicating high ligand/low receptor activity and *vice versa* for white cells. (a-c) Pattern formation under uniform signalling (Figure 4 (a)), and increasing R for (a) $R = 1$, (b) $R = 3$ and (c) $R = 6$. Isolated primary fate cells are selected in a field of secondary fate cells. For other parameters we set $\nu = 1$, $a = b = 0.01$, $h_1 = h_2 = 3$. (d-f) Pattern formation under targeted radial signalling (Figure 4 (b-c)), where in (d) to (f) we increase the target distance from the signalling cell. Specifically, we consider (6) with $\sigma_1 = 1$, $\sigma_2 = \alpha = \phi = 0, R = 10$ and (d) $\rho = 1$, (e) $\rho = 3$ and (f) $\rho = 6$. Blocks of primary fate cells are formed, surrounded by large regions of secondary fate cells. Other parameters are set at $\nu = 1$, $a = b = 0.1$, $h_1 = h_2 = 3$. For all simulations we consider a field of 75×75 cells and compute solutions until a (numerical) steady state distribution is achieved.

4.2.2. Radially asymmetric signalling

We next turn our attention to asymmetric signalling scenarios, as described in Section 3.1.2. Figure 10 illustrates the results from two simulation sets, as we shift from a symmetric to "axial" signalling scenario. Specifically we change the weighting function from radial uniform to restricted along a single axial direction: see Figure 10 (a-d, top panels) for the changing weighting function. The radial sym-

metric pattern is as above: isolated primary fate cells in a field of secondary fate cells. Biasing signalling in this manner results in variable spacing between primary fate cells according to the axial direction, culminating in single cell width primary fate stripes for the most extreme cases, see Figure 10 (d).

Next, we modulate the weighting function to shift from targeted/radially symmetric to targeted/axial signalling: see Figure 10 (e-h, top panels). Restricting the signalling towards a single axial direction now results in multi-cell width stripes, oriented along the direction of axial signalling.

5. Discussion

The hypothesis that cellular populations can perform direct cell to cell signalling across multiple cell lengths has gathered increasing momentum in recent years. Long, filopodia-like signalling protrusions (or cytonemes) have been observed in a variety of developing tissues and organs in distinct species, and are believed to have a potentially crucial role in their patterning and differentiation. In this paper we have developed a framework to model the impact of such cell to cell interactions, and subsequently explored how non-local contact based signalling can direct the emergence of pattern in a cellular field when operating in a lateral-inhibition type system. Specifically, we have expanded the well-established model of Collier *et al* [5] for juxtacrine-based lateral inhibition in the Delta-Notch system by permitting cells to signal directly at a distance, such that one cell can trigger action in another located multiple cell diameters away.

We used a combination of linear stability analysis and numerical simulation to investigate how the range and form of non-local signalling impacts on patterning. A key finding is that longer wavelength patterns develop in a robust manner which, according to the distribution of signal from the signalling cell, can vary from single isolated primary-fate cells to clusters and stripes; in contrast, the original model of Collier *et al* [5] tends to create fine-grained patterns. We note that longer wavelength patterns have been generated in other discrete-cell juxtacrine type mathematical models. Owen and Sherratt [18] observed multi-cell length patterns in a generalised model of nearest-neighbour signalling, however this required a lateral-induction (positive
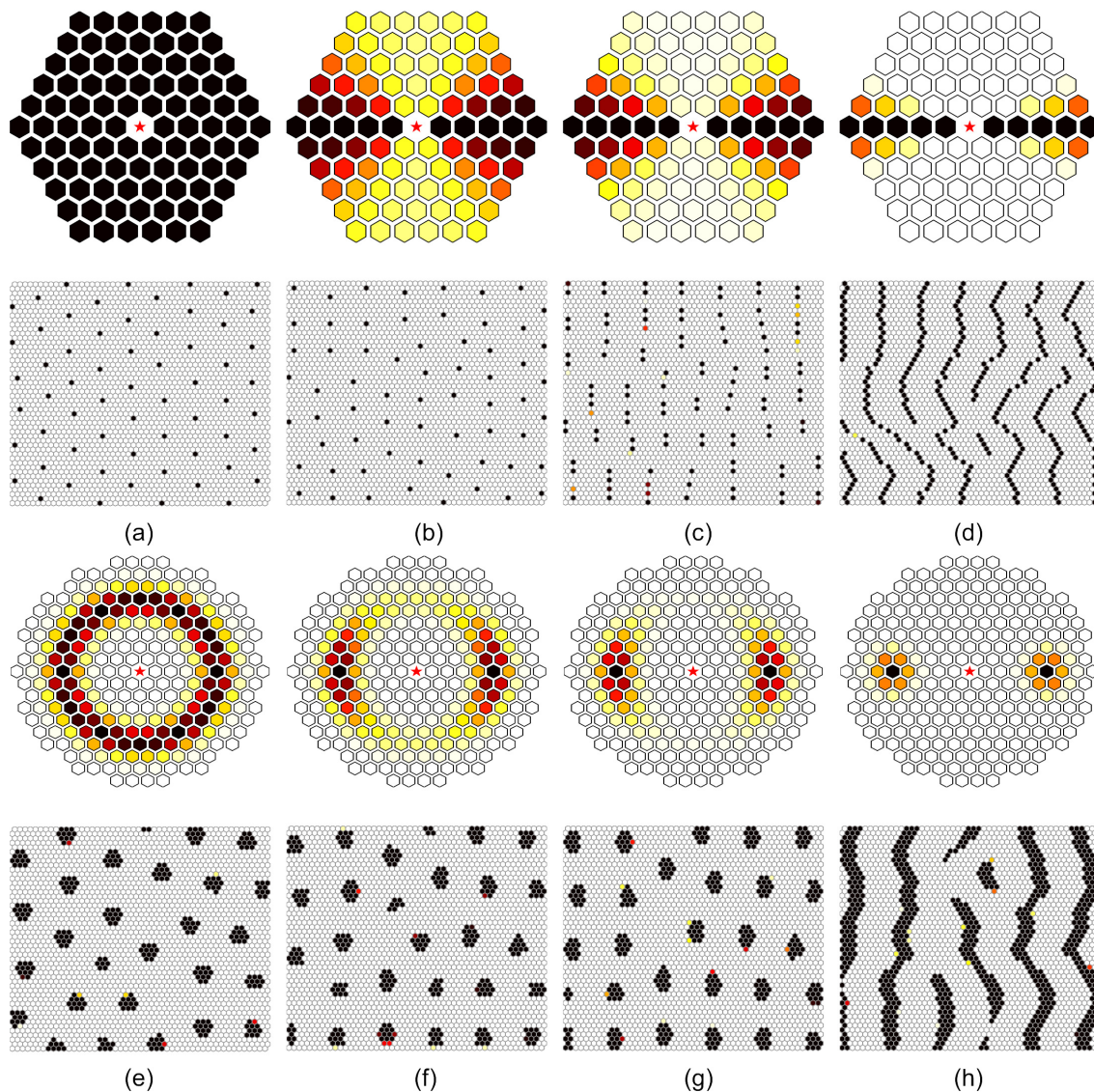
Figure 10: Transition from radially symmetric to axially oriented signalling scenarios. In each row as we move from left to right signalling is progressively shifted from radially symmetric to targetted along a specific axial direction. (Top row) All cells along a given axial direction are targetted: (a) $\sigma_2 = 0$; (b) $\sigma_2 = 1$; (a) $\sigma_2 = 2$; (b) $\sigma_2 = 10$. Other parameters are set at $R = 6$, $\alpha = 2$, $\sigma_1 = \rho = \phi = 0$. (Bottom row) Only a subset of cells along a given axial direction are targetted: (e) $\sigma_2 = 0$; (f) $\sigma_2 = 1$; (g) $\sigma_2 = 2$; (h) $\sigma_2 = 10$. Other parameters are set at $R = 8$, $\alpha = 2$, $\sigma_1 = 1, \rho = 5, \phi = 0$. Kinetic parameters are set at $\nu = 1$, $a = b = 0.01$, $h_1 = h_2 = 3$. For all simulations we consider a field of 75×75 cells and compute solutions until a (numerical) steady state distribution is achieved.

feedback) interaction between adjacent cells, instead of the lateral-inhibition mechanism of the Delta-Notch interaction. Chen and colleagues [2] extended the Delta-Notch model of [29] by incorporating a "Notch-gradient activity" term analogous to discretised diffusion, conferring a longer-range component to lateral inhibition. This model is successful is generating a sparser pattern, yet a precise mechanistic motivation for the added term is uncertain: the model presented here instead generates multi-wavelength patterns specifically through modelling the contribution from non-local cell-cell contacts.

Our findings specifically support those in [3], where a combined experimental/modelling approach was used to determine the role of filopodial-based interactions for the correct spacing between SOPs in Drosophila neoneurogenesis. Similar to here, they extended the model of Collier et al. [5] in non-local fashion, albeit with randomly distributed and dynamic filopodia to highlight the impact of the filopodial length and lifetime. A further analysis was performed in [4], where it was shown how noise and nonlocal contact-based signalling could generate a variety of pattern forms within a cellular automata based model for lateral inhibition. The work here differs in providing a more generalised and theoretical approach, allowing a comprehensive analysis into how various signalling scenarios will impact on the pattern form.

The use of the Collier et al. [5] model was practically motivated: it is simple and, as a pioneering model with well-known patterning properties, provides a logical point of reference. As previously mentioned, however, it suffers from certain drawbacks such as a degree of patterning sensitivity to environmental noise: we observe similar sensitivity here. More recent modelling by Elowitz and colleagues [29] has accounted for the impact of cis-inhibition of Notch and Delta in an extension of (1): significantly, their extended model resolves some of its shortcomings, demonstrating greater robustness and sharper transitions between upregulated/downregulated states. We have also performed simulations of the long-range direct contact signalling model here after replacing (1) with a Notch-Delta-cis interaction model of [29]: consistent patterning phenomena is observed (data not shown), suggesting that the patterns are not critically dependent on the precise form of the underlying equations. Nevertheless, a more formal exploration into how sensitive/robust the model is remains

a subject for future work.

It is also worth noting that the pattern change seen in, for example, Figures 10 (c) and (d) (or (g) and(h)) is quite significant given the relatively small variations in the corresponding spatial signal distribution. Given that environmental noise is expected to be considerable, and that an individual cell may not have such precise control over the extension and orientation of its filopodia, the robustness of such patterns is also an important point to consider. Incorporating the impact of environmental variability (e.g. via stochastically fluctuating signalling nets) would therefore be an important area for future studies. Of particular interest would be to additionally account for dynamic evolution of signalling nets according to the local and non-local contacts formed, and investigate whether this has the capacity to confer additional robustness to patterns.

Our linear stability analysis revealed that longer range signalling will typically place stronger constraints on the strength of feedback in the underlying molecular interactions: distributing to a wider field inevitably dilutes the ligand, and subsequently a stronger response must be generated. Yet, there is seemingly an upper limit to the feedback strength required: if feedback is sufficiently strong, patterning can potentially emerge for arbitrarily large signalling ranges. Of course, one must always view cautiously the results of linear analyses, and a non-linear study of the model provides an interesting direction for future research.

For practical reasons, the study here has been restricted to the analytically convenient case of fixed and homogeneous networks: even within this setting we can generate a broad variety of specific signalling nets and, subsequently, a wide range of patterns. In practice, patterning in embryos will typically takes place under a backdrop of considerable spatio-temporal complexity and relaxing further the restrictions here is likely to expand the range of patterning further. As an example, we illustrate via the preliminary simulations in Figure 11. Here we drop the homogeneous signalling net restriction, assuming instead that the weighting function changes with cell position in the field: from left to right, we assume signalling is increasingly shifted into more distant cells. Figure 11 (a) shows a pattern in which isolated
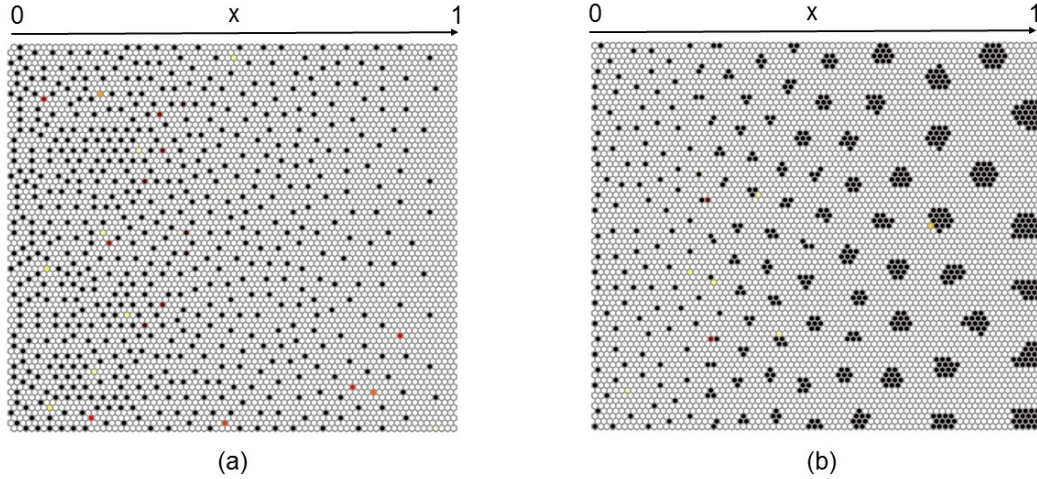
Figure 11: Patterning under heterogeneous signalling nets. In each simulation we allow the weighting function to vary such that, from left to right, the signalling becomes more concentrated into more distant cells. Note that for both cases the signalling nets are fixed and radially symmetric. Specifically, we consider (6) with: (a) $\sigma_1 = 2.5(1 - x)$, $\rho = 0$, $\sigma_2 = \alpha = \phi = 0$; (b) $\sigma_1 = 2.0$, $\rho = 1 + 5x$, $\sigma_2 = \alpha = \phi = 0$. Here, x represents the nondimensional coordinate along the horizontal axis, as shown. Kinetic parameters are set at $\nu = 1$, $a = b = 0.01$, $h_1 = h_2 = 4$ throughout on a field of 75×75 cells.

cells emerge, but with a spacing changing with axial position from fine to coarse grained. Figure 11 (b) illustrates a transition between fine grained isolated cells to coarsely grained clusters. While these simulations are preliminary, and designed to indicate the broader patterning capacity of the current model, an interesting focus for future studies would be to develop the model to investigate patterning within the context of a specific process of embryonic development, for example SOP specification, and where simulation results can be appropriately benchmarked against various experimental observations.

Appendix

The feedback strength $|AB|$ is controlled by parameters a, b, h_1, and h_2 in the feedback functions f and g, see Equations(2). Here we show the following result.

Lemma. Given the kinetics in equations (1), together with feedback functions (2)

for $a, b > 0$, and $h_1, h_2 \geq 1$, we have

$$|AB| < h_1 h_2 \,. \tag{12}$$

Proof.

First, we note that a single positive steady state (u_0, v_0) exists where

$$u_0 = \frac{v_0{}^{h_1}}{a^{h_1} + v_0{}^{h_1}} \quad \text{and} \quad v_0 = \frac{b^{h_2}}{b^{h_2} + u_0{}^{h_2}} \,. \tag{13}$$

We have $A = f'(v_0) = h_1 a^{h_1} \frac{v_0{}^{h_1-1}}{(a^{h_1} + v_0{}^{h_1})^2}$ and $B = g'(u_0) = -h_2 b^{h_2} \frac{u_0{}^{h_2-1}}{(b^{h_2} + u_0{}^{h_2})^2}$. Hence, after some manipulation,

$$|AB| = h_1 h_2 \frac{a^{h_1}}{b^{h_2}} \frac{u_0}{v_0{}^{h_1}} u_0{}^{h_2} v_0 \,. \tag{14}$$

The first equation in (13) implies $\frac{u_0}{v_0{}^{h_1}} < \frac{1}{a^{h_1}}$, while the second implies $u_0{}^{h_2} v_0 < b^{h_2}$. Taken together, we arrive at (12). $\square$

References

[1] S. J. Bray. Notch signalling: a simple pathway becomes complex. *Nat. Rev. Mol. Cell Biol.*, 7:678–689, 2006.

[2] J. S. Chen, A. M. Gumbayan, R. W. Zeller, and J. M. Mahaffy. An expanded Notch-Delta model exhibiting long-range patterning and incorporating Micro RNA regulation. *PLoS Comp. Biol.*, 10:e1003655, 2014.

[3] M. Cohen, M. Georgiou, N.L. Stevenson, M. Miodownik, and B. Baum. Dynamic filopodia transmit intermittent Delta-Notch signaling to drive pattern refinement during lateral inhibition. *Dev. Cell*, 19:78–89, 2010.

[4] M. Cohen, B. Baum, and M. Miodownik The importance of structured noise in the generation of self-organizing tissue patterns through contact-mediated cell–cell signalling *J. Roy. Soc. Interface*, 8:787–798, 2011.

[5] J. R. Collier, N. A. M. Monk, P. K. Maini, and J. H. Lewis. Pattern formation by lateral inhibition with feedback: a mathematical model of Delta-Notch intercellular signalling. *J. Theor. Biol.*, 183:429–446, 1996.

[6] F. Crick. Diffusion in embryogenesis. *Nature*, 1970.

[7] C. de Joussineau, J. Soulé, M. Martin, C. Anguille, P. Montcourrier, and D. Alexandre. Delta-promoted filopodia mediate long-range lateral inhibition in drosophila. *Nature*, 426:555–559, 2003.

[8] P. Formosa-Jordan and M. Ibañes. Diffusible ligand and lateral inhibition dynamics for pattern formation. *J. Stat. Mech.: Theor. & Exp.*, 2009:P03019, 2009.

[9] A. C. Gradilla and I. Guerrero. Cytoneme-mediated cell-to-cell signaling during development. *Cell & Tiss. Res.*, 352:59–66, 2013.

[10] K. G. Guruharsha, M. W. Kankel, and S. Artavanis-Tsakonas. The Notch signalling system: recent insights into the complexity of a conserved pathway. *Nat. Rev. Gen.*, 13:654–666, 2012.

[11] T. B. Kornberg and S. Roy. Cytonemes as specialized signaling filopodia. *Development*, 141:729–736, 2014.

[12] K. Mishra-Gorur, M. D. Rand, B. Perez-Villamil, and S. Artavanis-Tsakonas. Down-regulation of Delta by proteolytic processing. *J. Cell. Biol.*, 159:313–324, 2002.

[13] N.A.M. Monk. Restricted-range gradients and travelling fronts in a model of juxtacrine cell relay. *Bull. Math. Biol.*, 60:901–918, 1998.

[14] P. Müller, K. W. Rogers, R. Y. Shuizi, M. Brand, and A. F. Schier. Morphogen transport. *Development*, 140:1621–1638, 2013.

[15] J.D. Murray. *Mathematical biology: II. Spatial models and biomedical applications*. Springer, 3rd edition, 2003.

[16] M. S. Nielsen, L. Nygaard A., P. L. Sorgen, V. Verma, M. Delmar, and N. H. Holstein-Rathlou. Gap junctions. *Comp. Physiol.*, 2012.

[17] R. D. O' Dea and J. R. King. Multiscale analysis of pattern formation via intercellular signalling. *Math. Biosci.*, 231:172–185, 2011.

[18] M.R Owen and J.A. Sherratt. Mathematical modelling of juxtacrine cell signalling. *Math. Biosci.*, 153:125 – 150, 1998.

[19] M.R. Owen, J.A. Sherratt, and H.J. Wearing. Lateral induction by juxtacrine signaling is a new mechanism for pattern formation. *Dev. Biol.*, 217:54 – 61, 2000.

[20] E. Plahte. Pattern formation in discrete cell lattices. *J. Math. Biol.*, 43:411–445, 2001.

[21] E. Plahte and L. Øyehaug. Pattern-generating travelling waves in a discrete multicellular system with lateral inhibition. *Physica D*, 226:117 – 128, 2007.

[22] F.A. Ramirez-Weber and T.B. Kornberg. Cytonemes: cellular processes that project to the principal signaling center in Drosophila imaginal discs. *Cell*, 97:599–607, 1999.

[23] K. W. Rogers and A. F. Schier. Morphogen gradients: from generation to interpretation. *Ann. Rev. Cell & Dev. Biol.*, 27:377–407, 2011.

[24] S. Roy and T. B. Kornberg. Paracrine signaling mediated at cell–cell contacts. *Bioessays*, 37:25–33, 2015.

[25] N. M. Sherer and W. Mothes. Cytonemes and tunneling nanotubules in cell–cell communication and viral pathogenesis. *Trends Cell. Biol.*, 18:414–420, 2008.

[26] D. S. A. Simakov and L. M. Pismen. Discrete model of periodic pattern formation through a combined autocrine–juxtacrine cell signaling. *Phys. Biol.*, 10:046001, 2013.

[27] P. Simpson. Lateral inhibition and the development of the sensory bristles of the adult peripheral nervous system of Drosophila. *Development*, 109:509–519, 1990.

[28] D. Sprinzak, A. Lakhanpal, L. LeBon, J. Garcia-Ojalvo, and M. B. Elowitz. Mutual inactivation of Notch receptors and ligands facilitates developmental patterning. *PLoS Comp. Biol.*, 7:e1002069, 2011.

[29] D. Sprinzak, A. Lakhanpal, L. LeBon, L. A. Santat, M. E. Fontes, G. A. Anderson, J. Garcia-Ojalvo, and M. B. Elowitz. Cis-interactions between Notch and Delta generate mutually exclusive signalling states. *Nature*, 465:86–90, 2010.

[30] A. M. Turing. The chemical basis of morphogenesis. *Phil. Trans. Roy. Soc. Lond. B: Biol. Sci.*, 237:37–72, 1952.

[31] H.J. Wearing, M.R. Owen, and J.A. Sherratt. Mathematical modelling of juxtacrine patterning. *Bull. Math. Biol.*, 62:293–320, 2000.

[32] S.D. Webb and M.R. Owen. Oscillations and patterns in spatially discrete models for developmental intercellular signalling. *J. Math. Biol.*, 48:444–476, 2004.

[33] M. J. Wheelock and K. R. Johnson. Cadherin-mediated cellular signaling. *Curr. Opin. Cell. Biol.*, 15:509–514, 2003.

[34] L. Wolpert. Positional information and the spatial pattern of cellular differentiation. *J. Theor. Biol.*, 25:1–47, 1969.

[35] S. Zhou, W. C. Lo, J.L. Suhalim, M. A. Digman, E. Gratton, Q. Nie, and A. D. Lander. Free extracellular diffusion creates the Dpp gradient of the Drosophila wing disc. *Curr. Biol.*, 22:668–675, 2012.